SAND2010-6864C

# Differential Imaging Microscopy of Physically Complex Surfaces Undergoing Atmospheric Corrosion

*David G. Enos and Gerald R. Girard*
*Sandia National Laboratories*
*Albuquerque, NM 87185*

## ABSTRACT

Frequently, optical observation of component materials is the only viable technique to evaluate degradation processes *in-situ*. Unfortunately, due to the visually complex nature of many surfaces (*e.g.*, scratches, occlusions, etc.), the degradation process, particularly at early stages, is difficult or impossible to resolve. As a result, studies are limited to evaluating degradation well after initiation has taken place. Thus, there is a need for a technique that could be implemented utilizing image processing that allows the de-convolution of changes due to the degradation process of interest from the background "noise". An automated differential imaging system was constructed for *in-situ* studies of both aqueous and atmospheric environments to fulfill this need. The basic functionality of the Differential imaging system was demonstrated on gold plated copper and gold /nickel plated copper coupons exposed to a sulfide containing atmosphere.

## INTRODUCTION

Evaluation of the performance of connectors and other electronic components, and the construction of models to perform life prediction requires that the operative degradation mechanisms for a particular system be understood, and perhaps equally as important, be readily observable. Unfortunately, visual/optical observation of damage accumulation, particularly during the nucleation and early propagation stages, is often hindered by surface features and exposure environment. In order to observe and evaluate such degradation processes, one must be able to de-convolute the changes/response due to the degradation process from surface features and environment being evaluated (e.g., geometric complexities such as scratches, varying electroplate morphology, etc.). A key benefit of a sensitive, specimen independent in-situ optical (or other imaging method) technique for monitoring the evolution of degradation processes is the ability to extract time-dependent corrosion rate information. In-situ rate measurements are currently only available for a limited range of specimen configurations using indirect techniques to infer material loss. The technique developed through this research makes these measurements generically available for a wide range of specimen geometries and material/environment combinations undergoing atmospheric corrosion.

Differential image processing is a technique through which subtle, time-dependent changes in an object being imaged can be readily observed. In this technique, a series of high resolution images of the surface of interest are taken over a period of time, and then quantitatively compared to one another through image subtraction or some other similar post-processing method. Through this technique, the resulting image consists only of the changes that took place in the time between when the two images were acquired. Minute changes in the surface morphology not readily resolvable using traditional image analysis techniques can then be readily quantified. There are a number of key aspects of this technique that have been addressed in part via the work completed to date. One such area is image to image registry, a critical aspect of the technique – if the size scale of the features being characterized is at the sub-micron level, then the images must be aligned in both the X and Y directions at least that well. This becomes increasingly difficult as the magnification increases, or if multiple images must be taken to capture the region of interest then "stitched" together to form a complete image of the features of interest.

The basic functionality of the Differential imaging system was demonstrated on gold plated copper and gold /nickel plated copper coupons exposed to a sulfide containing atmosphere, model material/environment combinations simulating electrical connectors that have been heavily studied at Sandia,. The utility of the differential imaging technique was demonstrated by characterizing a series of different locations across a coupon surface as a function of time, requiring that both the X-Y position, as

well as the Z position (for focus) be precisely controlled. Future development of the hardware/software will enable the technique to be extended to complex surfaces (curved surfaces, etc.) as well as more thoroughly integrate image post processing algorithms.

## RESULTS

The differential imaging system consists of two primary components which may be broadly characterized as hardware and software. The hardware consists of the exposure chamber and sample positioning system, while the software consists of image acquisition and image processing modules. Each of these components will be discussed, followed by application of the differential imaging system to a specific material/environment combination.

*Gas Exposure System*

An overview of the current system configuration is presented in Figure 1. In order to allow automation of the magnification as well as the focusing process, the heart of the differential imaging system consisting of an automated variable imaging lens, that utilizes 5-phase stepper motors to control both magnification and focus. The lens also provides coaxial illumination utilizing an LED light source. By automating the magnification, the magnification and focus at the lens can be computer controlled via the system software discussed below. A long focal length objective lens is used to provide the high optical magnification required when observing surface degradation. While the motors in the lens have proven acceptable for coarse focus of the image, a precision linear stage is used for all focusing operations once an experiment is in progress. In addition to the stage used for fine focus, precision linear stages are also used for sample translation. All three stages are internally indexed, such that they can report their absolute position with a high degree of accuracy, an essential feature if stage movement errors/backlash effects are to be avoided.

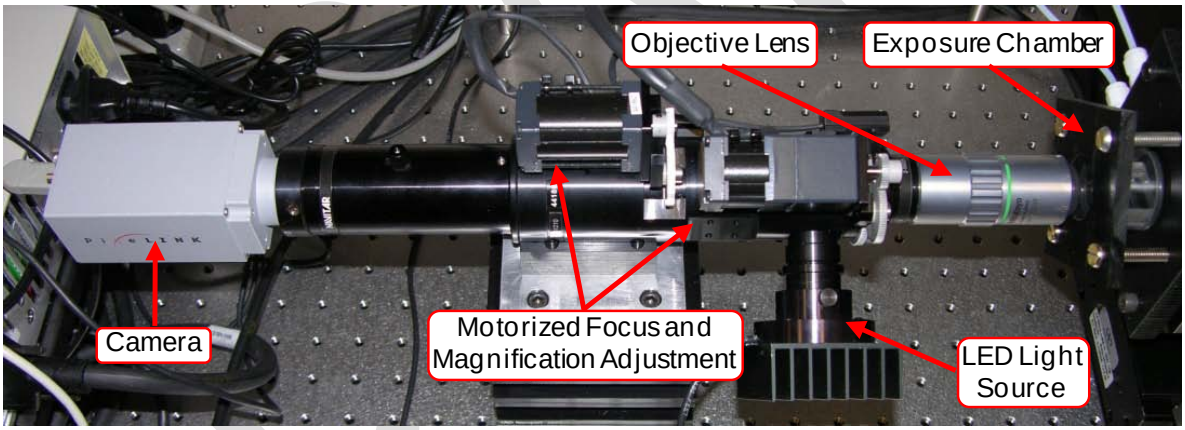


**Figure 1.** Photograph of the Differential Microscope System

The final physical aspect of the system is the exposure chamber itself. As illustrated in Figure 2, the exposure chamber has a gas inlet and outlet machined into the baseplate of the chamber. These provide a path for gas to flow to approximately the center of the exposure chamber. The top of the exposure chamber contains an AR coated glass window, allowing the specimen contained within the exposure chamber to be viewed at all times by the camera. The side of the chamber is polycarbonate, and allows for the use of a surface heater (not shown in the figure) – this is critical for high humidity environments where considerable condensation would take place if the chamber were not at temperature. Such condensation obscures the viewport and, more importantly, has a significant impact on corrosion processes. As such, the ability to prevent condensation by maintaining temperature control of the exposure chamber is a key design feature.

A

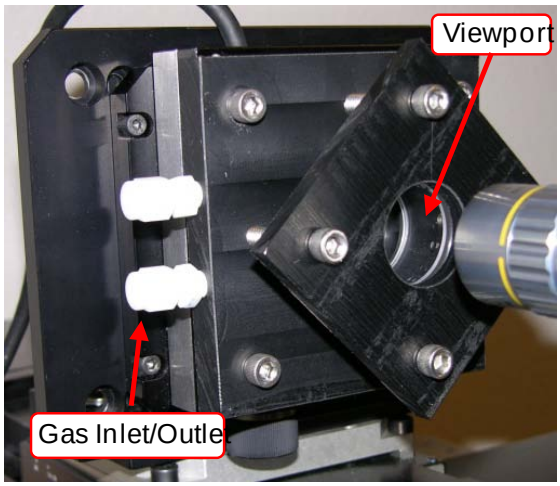


B

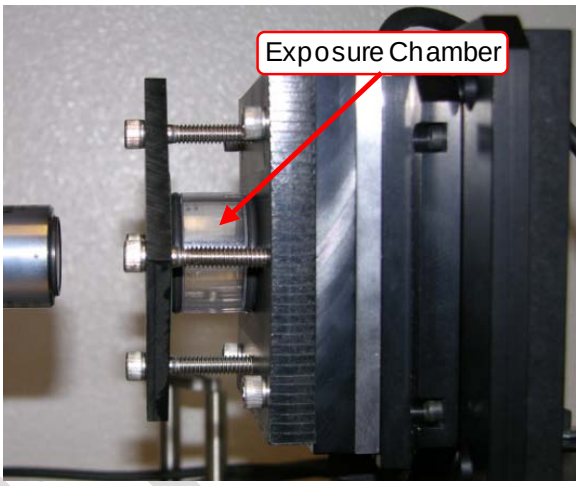


**Figure 2:** Environmental exposure cell allows for the flow through of a contaminant gas stream and optical monitoring of the sample via a viewport (shown in A). In addition, the side of the chamber (shown in B) can be wrapped with heat tape to allow for temperature control of the environment.

*Image Acquisition Software*

The image acquisition software is written in LabView, an object oriented, graphical programming environment. The software itself uses a parallel loop state machine design. The block diagram for this architecture, shown in Figure 3, has one while loop dedicated to handling image acquisition and the second loop assigned to differential image analysis. The multi-tasking design of parallel loops takes advantage of the multi-core microprocessor of the system computer. A state machine is a common design pattern for LabView applications and consists of a case structure embedded in a while loop, a shift register for passing the case selector value, and an enumerated type that contains the state names[1]. Each state corresponds to a different operation within the image acquisition loop. Use of this design simplifies both code readability and future modifications to the application program.

A key feature of the image acquisition software is the development and implementation of autofocus control. An autofocus system consists of two principal components – a means to measure the focus position and a quantitative assessment of focus quality. For measurement and control of the focus position, a motorized linear stage with an absolute positional control resolution of 0.1 microns is used. While the variable lens system has a 5 phase stepper motor to adjust the focus of the lens, it lacked the positional accuracy required for the differential imaging system

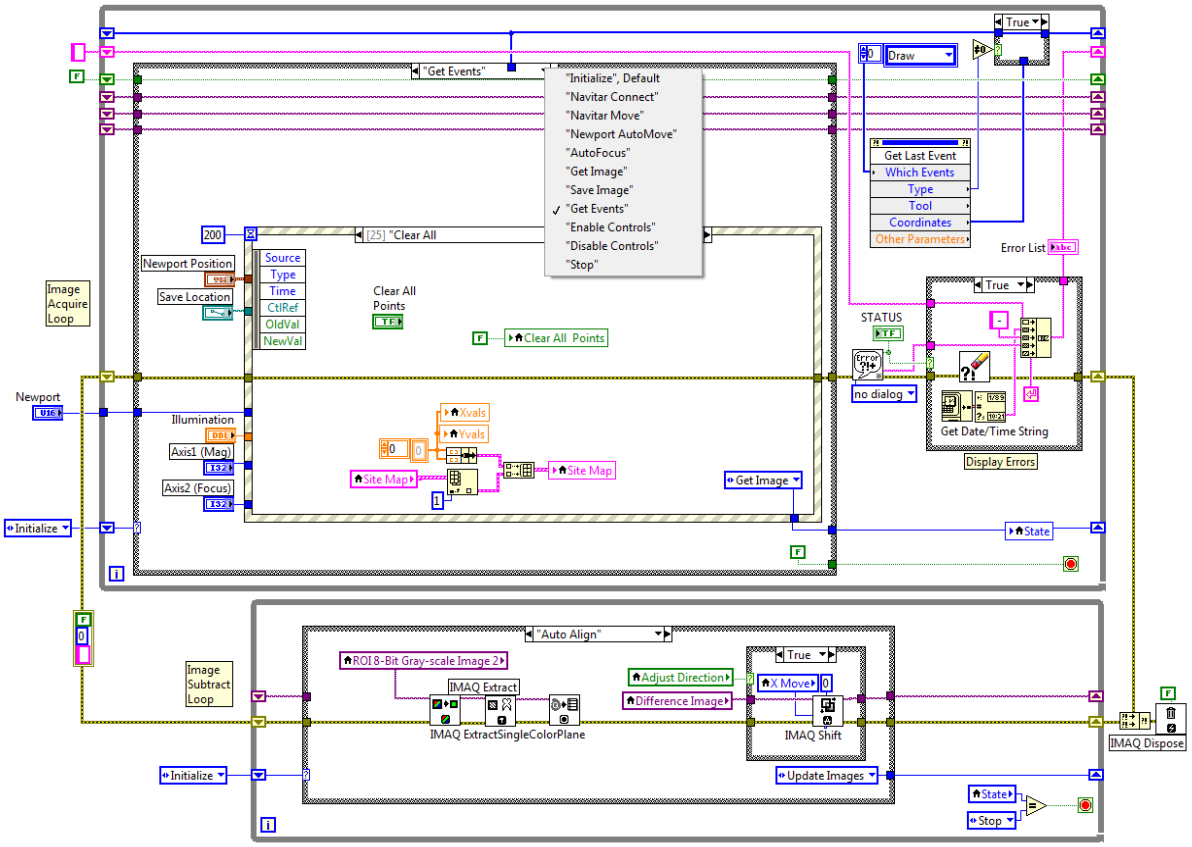


**Figure 3.** The image capture LabView software block diagram. Parallel loops are used for image acquisition and image subtraction, each loop operating as a state machine. The image acquisition loop contains an event handler for processing user requests from the graphical user interface.

The autofocus routine itself implements a 2 stage focusing method. First, a coarse focus is executed with large (1 to 3 microns) step size using the histogram contrast method for measuring focus quality. Although the histogram algorithm may be the best method for focusing a blurred image, the limited depth of field of the microscope (typical for high magnification objective lenses) still requires the starting sample position be within 30 microns to determine the correct direction for focus position adjustment. After focus position is determined to within a few microns, a fine focus algorithm with a finer step size (0.1 to 0.5 microns) is executed. The user may select to operate the final focus using either the histogram or edge detection method for determining image sharpness.

The mapping capability of the software was expanded to include 100 sites per sample and a grid map display of sites. A graphical interface is used to illustrate the location of the sites selected by the user, as illustrated in Figure 4. The location of each measurement site is indicated with white dots within a red border polygon indicating the test sample perimeter. The user interface allows sites to be added, removed, or selected for motorized stage navigation.

The last feature of the image acquisition application is an integrated differential image analysis tool. Although a simplified version of the standalone application (which will be discussed in the next subsection), the differential image analysis tool in the main program (see Figure 5) enables users to either determine the difference between two previously saved images or to compare a live image to a previously saved one. A detailed discussion of the differential image software follows in the next section.

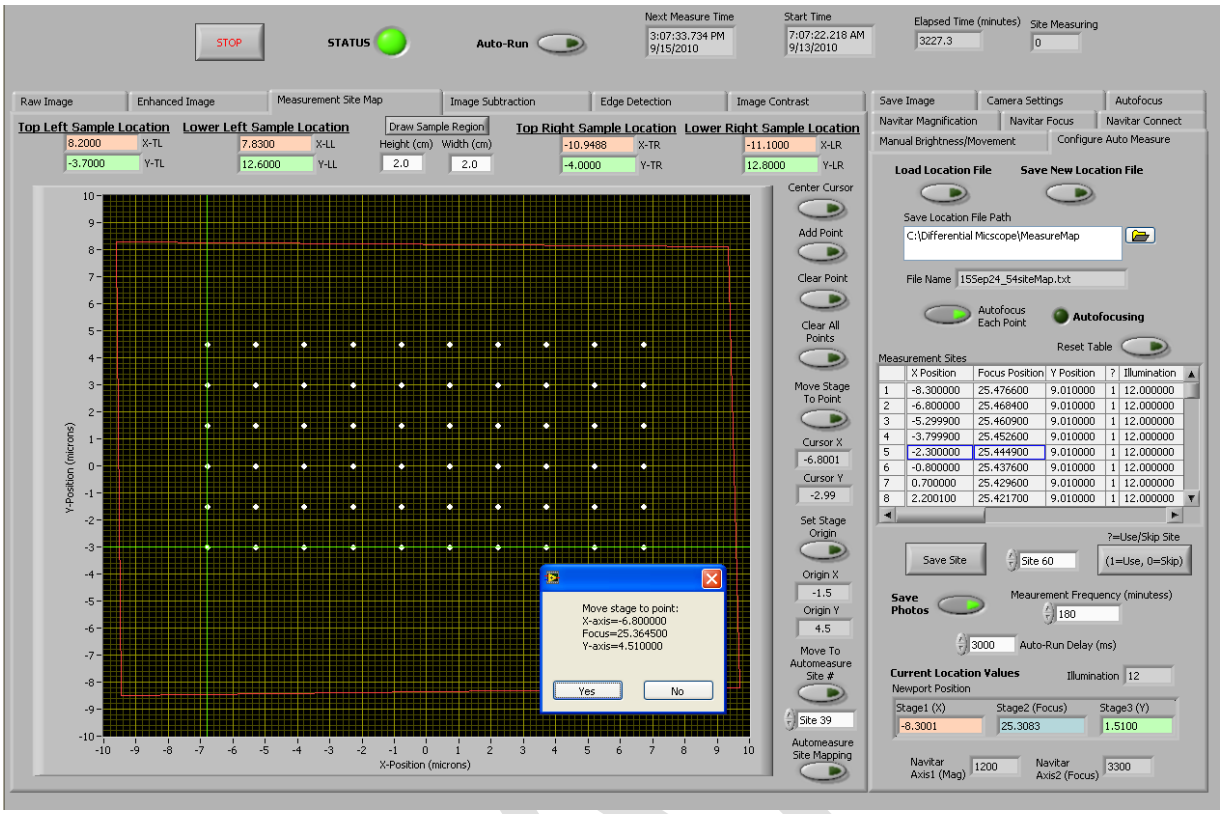


**Figure 4.** The image capture program has been updated to included site mapping of up to 100 sites per sample. A point-and-click user interface is available for navigation across the sample surface and display of site locations on a grid map.

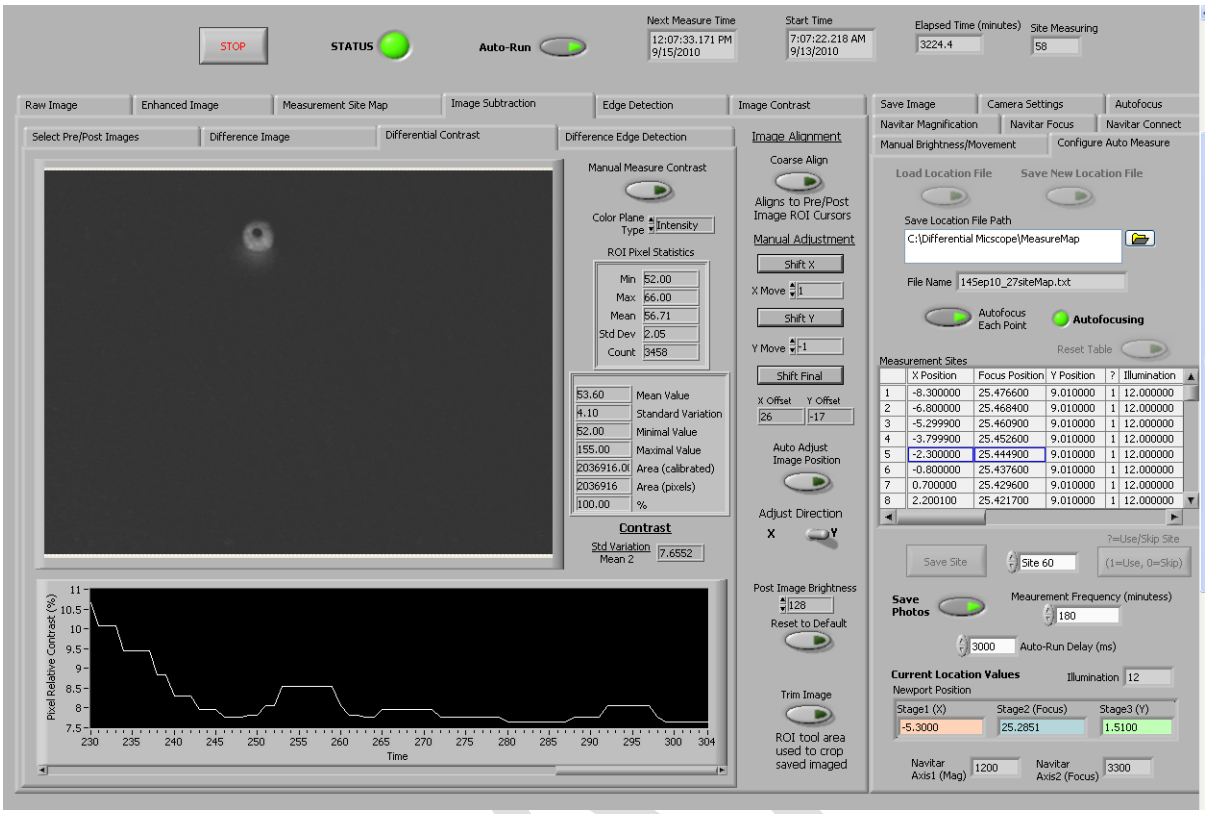


**Figure 5.** Another capability added to the image capture software is integrated image subtraction, including comparison of a live image to a previously saved baseline.

*Image Analysis Software*

As indicated above, two software tools were developed for creating and analyzing difference images. The primary analysis tool exists as a standalone application, while the secondary is a module accessible within the main image acquisition program. The NI Vision Development Module created a difference image through matrix subtraction of the intensity values from two images[2].

Figure 6a shows the image selection tab window for pre and post saved images. A coarse alignment tool is available that provides point and click selection of identical locations on each image and performs a first order alignment. To match pre and post image brightness, image brightness adjustment and luminance measurement are also provided.

Figure 6b shows the resultant difference image and includes some image utilities. An image reversal option is provided to change the order of pre and post image subtraction, highlighting any found differences. Differential image brightness, contrast, and gamma adjustment are also available. A defect site measurement tool is also present for estimating the cross sectional area of a defect observed within the main image. Once constructed, the differential image may be saved as either the entire image area or a user defined ROI area. A tabular summary of saved images (Figure 6d) is available and may be saved as a text file.

One challenge for accurate image subtraction is precise alignment of the two images that are being compared, as misalignment will result in visible features within the difference image that are not the result of corrosion. Accurate alignment of the pre and post images requires that the contrast of the difference image be minimized. Scratches and other surface features present in both pre and post images should cancel each other out during the subtraction calculation. Figure 6c shows an edge detection measure tool provided for measuring image alignment, in addition to the histogram contrast

measurement tool previously shown in Figure 5. A semi-automated X and Y axis alignment tool is used to shift the images relative to one another in order to match pre and post images as closely as possible.

a

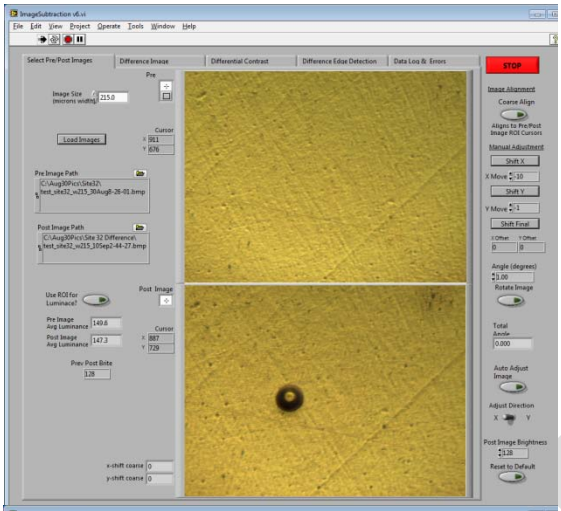

b

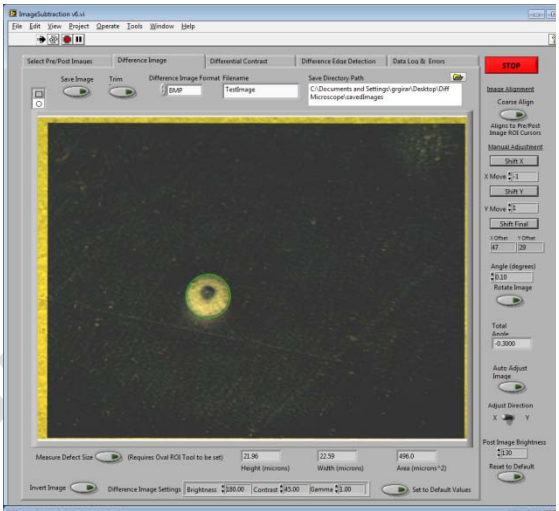

c

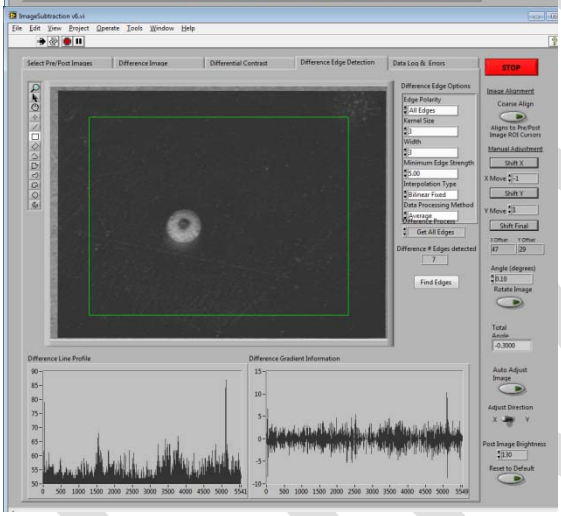

d

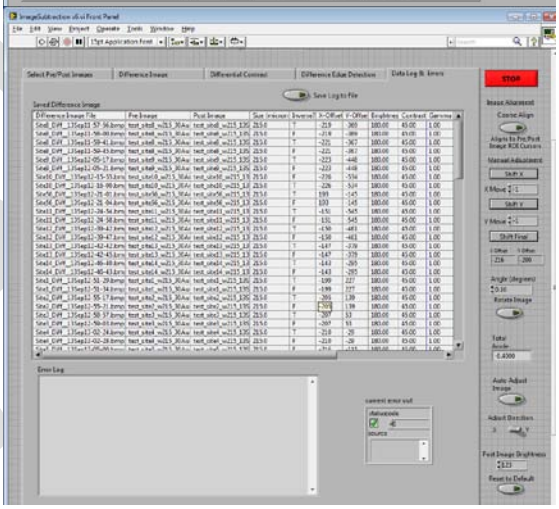

**Figures 6a-d.** Four screen views of the image subtraction processing and analysis software. (a) Pre and post image selection and coarse alignment. (b) Composite subtracted image with defect size measurement capability. (c) Subtracted image contrast and edge detection measurement for determination of pre to post image fine alignment. (d) Summary table of saved subtracted images.

*Demonstration of Basic System Functionality*

Data taken from automated measurements on an oxygen free copper coupon that had been electroplated with 2.5 microns of gold on top of a 5 micron nickel layer was used to demonstrate the capabilities of the Differential Imaging system. Data was acquired over several weeks with the sample exposed to a Battelle Class 2 mixed flowing gas environment. Example analyses of difference images and cross sectional area changes for two representative defects are shown in Figures 7 and 8. Difference images were acquired for a series of sixty discrete predetermined locations across the sample surface at 1 hour time intervals over a 2 week period. Figure 7 shows the development of a corrosion site that nucleated at the start of gas flow. After a brief initial growth period, the site remained fairly constant in size for 10 days, at which point the site grew rapidly and then passivated again. During the second growth period, the defect site grew approximately 3 times larger in size.

Although many corrosion sites were visible shortly after starting gas flow, some corrosion sites took more than one week to appear. Shown in Figure 8 is one such site with delayed growth that also shows the same two step growth pattern of 1st and 2nd passivation stages. These difference images and plots of measured cross sectional area versus time are examples of the capability of the system to detect and quantitatively measure corrosion site growth. Moreover, although these difference images are a comparison of pre and post exposure to corrosive gasses, pre and post images may be compared for any two time periods of interest including a comparison between two different phases of corrosion growth.

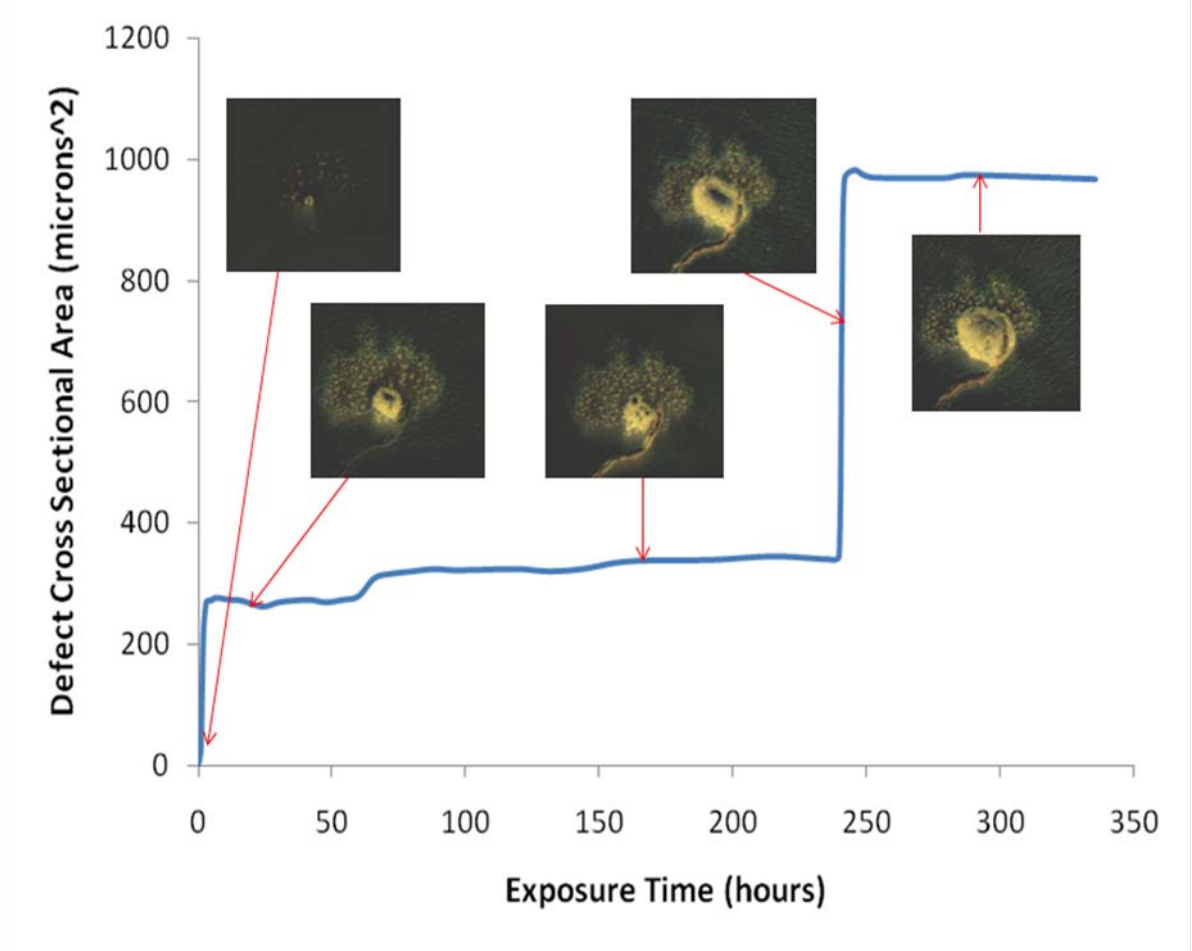


**Figure 7.** Corrosion site area measurements of differential images showing the change in defect size and appearance over a two week time period (image size is 60 x 75 microns). This defect grew at the onset of exposure to corrosive gasses and did not complete second passivation until 10 days later.

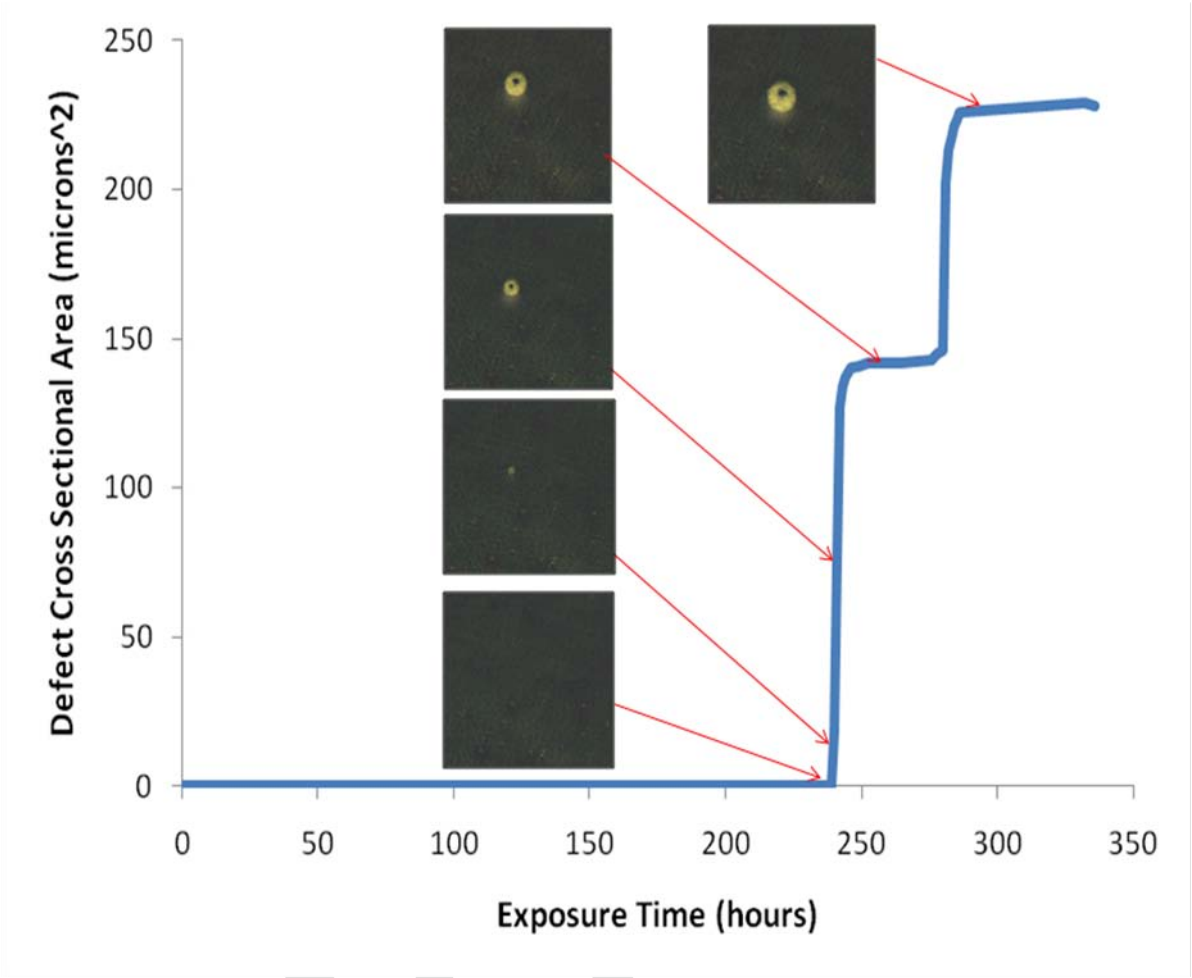


**Figure 8.** Corrosion site area measurements of differential images showing the change in size and appearance of a defect not visible until 10 days after exposure (60 x 75 microns image size).

Despite extensive effort both at and external to Sandia to elucidate the mechanisms of sulfidation corrosion of copper and Au-plated copper, much remains unknown. This is demonstrated by the observations presented in Figures 7 and 8, specifically the observation that corrosion sites initiate and grow, then appear to stifle/passivate, only to grow again at a later time has not been observed experimentally previously, nor has it been reported in the literature. This phenomenon was not observed on specimens that did not have a nickel underplate, suggesting it may be related to the presence of that layer. However, care must be taken in drawing conclusions at this point due to the limited dataset that is presently available. That being said, as reported in Enos (2010)[3], there are two phenomena that may have led to this behavior. In specimens with the nickel underlayer, some sites were observed where corrosion was confined to the nickel layer, while in others it had progressed into the underlying copper. Once corrosion reached the copper, a significantly larger quantity of corrosion product migrated to the gold surface. It is possible that the second growth stage represents the point at which the nickel layer is breached, resulting in the large increase in corrosion site size presented in Figures 7 and 8. Another phenomenon that may have lead to this observation is the deformation of the gold layer which has been observed in coupons with a nickel underplate. As corrosion progresses, corrosion product builds beneath the gold layer, resulting in the formation of a blister. At this point, growth of the corrosion product is physically constrained by the gold, which may give the appearance of the site passivating/stifling. Eventually, the gold layer ruptures, resulting in a large quantity of corrosion product transporting to the gold surface that could also appear as the second growth stage presented in Figures 7 and 8. As cautioned above, the observation of additional samples is necessary, combined with other analysis

techniques such as the focused ion beam cross sectional analyses presented in Enos, 2010[3], before any conclusions as to what is actually taking place can be made.

The ability to detect corrosion sites of a few microns size was another capability demonstrated by the differential imaging system in FY10. Figure 9a and Figure 9b show the growth of a small corrosion site that is barely discernable when viewing the pre and post images from exposure to corrosive gasses. Differential image analysis shows a small defect site that is visible as a bright spot in a black background (Figure 9c). Increasing the image size by 5X sand providing a scale for dimensional reference shows the defect to be 3 microns diameter (Figure 9d).

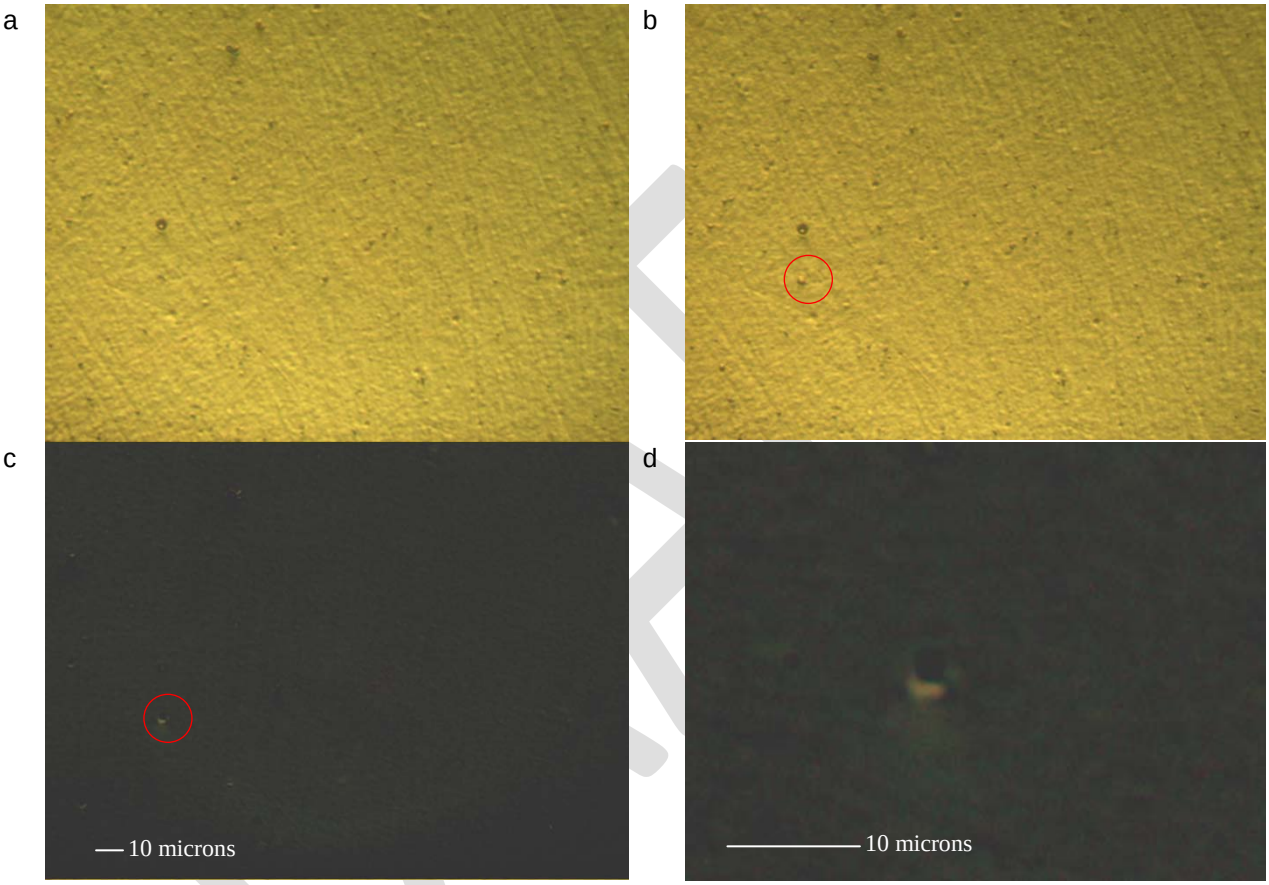


**Figures 9a-d.** Differential image detection of subtle changes to a measurement site of 161 x 215 microns size. Pre (a) and post (b) images of a surface that appears nearly identical except for a small change that is circled in red. Image subtraction (c) of the two images highlights this difference. Zooming in to the defect site at 5 times greater magnification (d) shows the defect to be 3 microns diameter.

## CONCLUSIONS

- An automated system has been developed that contains all of the tools to monitor atmospheric corrosion kinetics in-situ. Difference imaging, the primary analysis routine in this system, has been successfully used to observe and measure corrosion processes which are difficult, if not impossible, to track via other methods.

- Application of the differential imaging technique to electronic connector materials has yielded new insights into the corrosion process. While additional work is necessary before conclusive statements

can be made, it is clear that the corrosion process is more complex than has been reported previously both by internal research as well as in the open literature.

- Through the use of this system, a more effective, unbiased means to assess the statistical distribution of corrosion sites on a gold plated (with a nickel underplate) copper surface over time. This understanding is critical if effective models of degradation of this material (for connectors, etc.) are to be formulated.

## ACKNOWLEDGEMENTS

Sandia National Laboratories is a multi-program laboratory managed and operated by Sandia Corporation, a wholly owned subsidiary of Lockheed Martin Corporation, for the U.S. Department of Energy's National Nuclear Security Administration under contract DE-AC04-94AL85000.

## REFERENCES

[1] Peter A. Blume, *The LabView Style Book*, Prentice Hall, 2007.

[2] Christopher G. Relf, *Image Acquisition and Processing with LabView*, CRC Press, 2004.

[3] D.G. Enos "*Understanding the Atmospheric Degradation of Noble Metal Plated Connector Materials*", Corrosion Journal Vol. 66, no. 10 (2010) SAND2010-3033J